Supporting Information

Interpretation of NO_3-N_2O_5 observation via steady state in high aerosol air mass: The impact of equilibrium coefficient in ambient conditions

Xiaorui Chen[1], Haichao Wang[3,4], Keding Lu[1,2]

[1]State Key Joint Laboratory of Environmental Simulation and Pollution Control, College of Environmental Sciences and Engineering, Peking University, Beijing, China.

[2]The State Environmental Protection Key Laboratory of Atmospheric Ozone Pollution Control

[3]School of Atmospheric Sciences, Sun Yat-sen University, Zhuhai, 519082, China

[4]Guangdong Provincial Observation and Research Station for Climate Environment and Air Quality Change in the Pearl River Estuary, Key Laboratory of Tropical Atmosphere-Ocean System, Ministry of Education, Southern Marine Science and Engineering Guangdong Laboratory (Zhuhai), Zhuhai, 519082, China

Correspondence to: Haichao Wang (wanghch27@mail.sysu.edu.cn), Keding Lu (k.lu@pku.edu.cn)

Contents

Supplementary Text:

Text S1. Ambient case invalid for NO_3-N_2O_5 steady state analysis

Text S2. Observation datasets from field campaigns 2017PKU and 2018TZ

Text S3. Characteristic of nighttime NO_3-N_2O_5 loss pathway in half-artificial dataset

Text S4. Parameterization of Keq coefficient in different databases

Text S5. Sensitivity tests of time to approach steady state

Text S6. The impacts of $k$$NO_3$ and $k$$N_2O_5$ levels on $\gamma_{ss}(N_2O_5)$

Supplementary Figures: Figure S1 to Figure S9

Supplementary Tables: Table S1 to Table S4

References

S1. Ambient case invalid for NO_3-N_2O_5 steady state analysis

Take two typical cases in winter and summer respectively for example to illustrate the conditions under which steady state analysis is invalid for interpreting NO_3-N_2O_5 observation and deriving $\gamma(N_2O_5)$. Over the period of wintertime case shown in Figure S1, the NOx and Sa concentration were low inferring a clean episode. Albeit the correlation coefficient for deriving $\gamma(N_2O_5)$ by steady state approximation appears to be high, an unreasonably negative $k$$NO_3$ value of this analysis period from the slope (Figure S1d) indicates that the steady state in this case still requires much longer induction time due to low strength of NO_3-N_2O_5 sink. In summertime case, although large sink rate contributed to fast approach of steady state, frequent injection of NOx emission could significantly modify the air mass condition. Less than enough time for mixing and reacting due to emissions deviates the air mass from steady state, resulting in weak correlation of steady state parameters (Figure S1e-h).

S2. Observation datasets from field campaigns 2017PKU and 2018TZ

The datasets used for analysis in this study were obtained from two field campaigns with different ambient conditions. The PKU2017 winter campaign took place from mid-November to late-December 2017 in the campus of Peking University, which is at urban area of Beijing, China. And the other one TZ2018 summer campaign took place from late-May to mid-June 2018 at a suburban supersite, Taizhou, China. More specific information about these two campaigns can be referred to our previous studies (Ma et al., 2019;Wang et al., 2020), while only basic background of site location and analysis-relevant instrumentation are provided below.

During the PKU2017 campaign, all instruments were applied on the roof of building in the campus of Peking University, which was about 100 m west to the major roads with strong influence of vehicle emissions. Each sampling inlet was distributed at least 20 m above the ground. The strong northerly winds with dry and clean air mass during the winter would periodically transport to this site, bring in fresh O_3 at night. The TZ2018 site is surrounded by agricultural land and fishponds, resulted in strong influence of biogenic emissions and occasional biomass burning. Each sampling inlet was distributed about 5 m above the ground. It should be noted that low concentration level of NO was frequently observed at this site due to a major highway within 0.5 km.

Same instrumentation was implemented in these two campaigns, and the related information are given in Table S1. Since the NO_3-N_2O_5 chemistry appears to be relatively sensitive to NO concentration, we corrected the nighttime NO data near the detection limit with mean values during the period of O_3 concentration higher than 25 ppbv.

S3. Characteristic of nighttime NO_3-N_2O_5 loss pathway in half-artificial dataset

The validity of NO_3-N_2O_5 steady state depends on their atmospheric lifetime, in other words their loss rate constants (Brown et al., 2003). In different seasons or areas, variations of emission, temperature, and other relevant factors can sufficiently change the sink strength of ambient NO_3 and N_2O_5 and thus relative occupations of these pathways. As half-artificial datasets (detailed in Methods) indicated, the average nighttime loss rate of NO_3 and N_2O_5 at PKU site in winter were 41 pptv h^{-1} and 195 pptv h^{-1}, whereas much higher rates were obtained at TZ2018 campaign with 451 pptv h^{-1} for NO_3 and 390 pptv h^{-1} for N_2O_5. Distinguished from a dominant sink rate of N_2O_5 in winter, total sink rate attribution shifted to NO_3 side in summer with significant larger sink strength than that in winter. The average proportions of NO_3 and N_2O_5 removal in each night is shown in Figure S2, where the nights with missing data represents that there is less than 15% valid data. Under the condition of approximate steady state, the sink flux contributed through N_2O_5 reaches up to 55~95% in wintertime campaign 2017PKU with an average higher than 80%, whilst it turns out to be less than 50%, even 5%, in 2018TZ summer campaign. Besides the different emission compositions at these two sites leading to significant distinction of removal attribution (strong biogenic emission at TZ site and high anthropogenic emission at PKU site), high temperature during summer facilitates the equilibrium in reactions R1 shifting to NO_3, further increasing the sink flux of NO_3. The attribution of removal pathways among NO_3 and N_2O_5 directly determines the weights of two terms on the right side of steady state expressions Eq. (1) and Eq. (2), contributing to assessing the impacts of several variables on steady state fitting among different reactivity conditions.

Taking two typical cases from these two datasets for example, the N_2O_5 lifetime was about 20 minutes in winter (Figure S3(a)), while was largely reduced to 100 seconds for summertime case (Figure S3(c)). Significantly different atmospheric lifetime for these two cases was majorly resulted from varying uptake removal pathways instead of $k$$NO_3$ from gas-phase reactions. Higher humidity at TZ site during nights facilitated hygroscopic growth of particles, the Sa concentration of which usually increased up to thousands of $\mu m^2\ cm^{-3}$ promoting the uptake reactions of NO_3 and N_2O_5, whereas Sa in the PKU site case become lower than 500

μm^2 cm^{-3} under the impact of clean and dry air mass. The steady state lifetime denoted by blue dash line in Figure S3(a)&(c), shows good agreement with atmospheric lifetime in both of cases, indicating that the NO_3-N_2O_5 chemical system simulated by steady state model is validated to be approximate steady state (deviation <5%). However, even in these cases, the derived uptake coefficient of N_2O_5, $\gamma_{ss}(N_2O_5)$, through steady state fitting (Figure S3(b)&(d)) still have a significant bias (>20%) from the setting values 0.02. Furthermore, we found that unexpected difference between $\gamma_{ss}(N_2O_5)$ fitting results and $\gamma(N_2O_5)$ setting values is common for all selected steady state periods in datasets. Since the influence of covariance of Sa and Keq$\times$[NO_2] has been avoided by applying Eq. (2) (Brown et al., 2009), the bias of $\gamma_{ss}(N_2O_5)$ presented in the above fitting calculation could be produced by interaction between equilibrium and steady state, variation of relevant parameters in the fitting equations (such as $k$$NO_3$, $k$$N_2O_5$, etc), which are discussed in the main text.

S4. Parameterization of *K*eq coefficient in different databases

*K*eq of NO_3-N_2O_5 system is a temperature dependent parameter, which has been extensively quantified in the laboratory (Pritchard, 1994). According to simultaneous measurements of N_2O_5, NO_3 and NO_2 concentration in a reaction chamber, the *K*eq can be directly calculated (Cantrell et al., 1988;Graham and Johnston, 1978;Osthoff et al., 2007), while the measurements of k_{R1a} and k_{R1b} or other accompanied parameters provides indirect ways to quantify *K*eq (Cantrell et al., 1993;Kircher et al., 1984;Smith and Ravishankara, 1985). However, distinct differences arise from these *K*eq results, which might be ascribed to the calibration uncertainty of absorption cross sections of NO_3 and NO_2 molecule (Osthoff et al., 2007). Jet Propulsion Laboratory (JPL) database provides an empirical formula, similar with Arenius formula, to calculate *K*eq in a simple way:

$$K_{eq} = A \times \exp(B/T), \quad \text{(S1)}$$

Here T denotes ambient temperature, and coefficients A and B are empirical parameter derived from laboratory works. Nevertheless, only parameterizations of k_{R1a} and k_{R1b} based on fall-off curve are described in IUPAC database and most of chemical mechanisms, without a direct formula to estimate *K*eq value.

Here, a set of uniform formulas are applied to describing k_{R1a} and k_{R1b}, capable of reproducing the preferred values given by several popular atmospheric chemistry mechanisms (Mozart, CB05, Saprc07, RACM2 and kinetic databases JPL2015 as well as IUPAC2017) and finally calculating *K*eq. As shown in Eq. (S2) and Eq. (S3):

$$k_{R1a}([M],T) = \left(\frac{k_O(T)[M]}{1+\frac{k_O(T)[M]}{k_\infty(T)}}\right) \times F^{\left\{1+\left[\frac{log_{10}\left(\frac{k_O(T)[M]}{k_\infty(T)}\right)}{g}\right]^2\right\}^{-1}}, \quad \text{(S2)}$$

$$k_{R1b}([M],T) = \left(\frac{\frac{k_O(T)[M]e^{\frac{-B1}{T}}}{A}}{1+\frac{k_O(T)[M]e^{\frac{-B1}{T}}}{k_\infty(T)e^{\frac{-B2}{T}}}}\right) \times F^{\left\{1+\left[\frac{log_{10}\left(\frac{k_O(T)[M]e^{\frac{-B1}{T}}}{k_\infty(T)e^{\frac{-B2}{T}}}\right)}{g}\right]^2\right\}^{-1}}, \quad \text{(S3)}$$

The parameter [M] represent molecular density in ambient air. $k_o(T)$ and $k_\infty(T)$ are rate coefficients of third-body reactions under low and high pressure respectively, which over different temperatures can be extrapolated by Eq. (S4) and Eq. (S5) based on 300 K measurement or simulation results:

$$k_o(T) = k_o^{300}\left(\frac{T}{300}\right)^{-n}, \quad \text{(S4)}$$

$$k_\infty(T) = k_\infty^{300}\left(\frac{T}{300}\right)^{-m}, \quad \text{(S5)}$$

All parameters in the above formulas are summarized in Table S3 and Table S4, which can be applied to calculating *K*eq coefficient via k_{R1a}/k_{R1b}. We found that there are significant differences among the parameters from these chemical mechanisms and databases, with a maximum discrepancy of 63% propagating to *K*eq at 298 K.

S5. Sensitivity tests of time to approach steady state

In Figure S7 and Figure S8, a series of sensitivity test provide an assessment of the time a valid steady state needs under several conditions. The most sensitive variables to approaching steady state are $k\mathrm{N_2O_5}$, $k\mathrm{NO_3}$ and T, the enhancement of which reduces the induction time, facilitating the valid steady state of $\mathrm{NO_3}$-$\mathrm{N_2O_5}$ system. In the case of increasing $k\mathrm{N_2O_5}$ and $k\mathrm{NO_3}$, the fast approaching to stead state is accounted by lower concentration of $\mathrm{NO_3}$ and $\mathrm{N_2O_5}$ when the steady state is valid. By comparing the sensitivity tests based on summertime (Figure S7(a)) and wintertime (Figure S7(b)) conditions, the impacts of $k\mathrm{N_2O_5}$ on approaching steady state is found to be more efficient than that of $k\mathrm{NO_3}$ in winter, while both contribute similarly in summer.

The different sensitivities to their reactivity in different seasons could be determined by the weights of loss pathways (Text S3). During the winter, such as the condition of PKU2017, the $\mathrm{N_2O_5}$ usually accounted by over 80% of the overall loss frequency of $\mathrm{NO_3}$-$\mathrm{N_2O_5}$ system, leading to high sensitivity to $k\mathrm{N_2O_5}$, while comparable loss frequency was occupied by both of $\mathrm{NO_3}$ and $\mathrm{N_2O_5}$ during the summer. As for the temperature, lower temperature shifts the equilibrium in R1 to $\mathrm{N_2O_5}$ side, which delay the time for developing equilibrium. By contrast, enhanced loss through $\mathrm{NO_3}$ with higher ambient temperature decreases the influence of equilibrium, boosting the approach to steady state. Moreover, Figure S8 shows relatively weak sensitivity of $\mathrm{NO_2}$ and $\mathrm{O_3}$ concentration to steady state approach. While changing $\mathrm{O_3}$ concentration barely contribute to promote a valid steady state in the scenario of this analysis, the $\mathrm{NO_2}$ concentration shows a positive sensitivity in some cases. Like the ambient temperature, changing $\mathrm{NO_2}$ concentration could shift the ratio of $\mathrm{N_2O_5}/\mathrm{NO_3}$ when steady state is valid and thus the time it requires. Especially under the condition of low ratio of $\mathrm{NO_2}$ to $\mathrm{O_3}$, like that in TZ2018, the enhancement of $\mathrm{NO_2}$ concentration shift $\mathrm{NO_3}$ to $\mathrm{N_2O_5}$ production and amplify the influence of equilibrium reactions. Instead, with a sufficiently high ratio of $\mathrm{NO_2}/\mathrm{O_3}$, the loss associated with $\mathrm{NO_3}$-$\mathrm{N_2O_5}$ system has been already dominated by $\mathrm{N_2O_5}$ removal, eliminating the influence of $\mathrm{NO_2}$ increase on delaying steady state. Previous research has also found similar trends of time to develop steady state according to simple scenarios simulated

by box model (Brown et al., 2003).

S6. The impacts of $k\mathrm{NO_3}$ and $k\mathrm{N_2O_5}$ levels on $\gamma_{ss}(\mathrm{N_2O_5})$

In order to demonstrate the impacts of $k\mathrm{NO_3}$ level on deriving $\gamma_{ss}(\mathrm{N_2O_5})$, another three half artificial data set are formulated through steady state model also based on the same observational constraints with $k\mathrm{NO_3}$ levels increased to 3 times (Mod1), 6 times (Mod2) and 10 times (Mod3) respectively, while other parameters remained unchanged. Similarly, the steady state fitting is used to obtain $\gamma_{ss}(\mathrm{N_2O_5})$ for each 2-hour time-period as Mod0. The mean discrepancy from complete steady state of these time periods and the median deviation of derived $\gamma_{ss}(\mathrm{N_2O_5})$ from pre-set $\gamma(\mathrm{N_2O_5})$ are shown as solid circles and triangles in Figure S9. With the enhancement of $k\mathrm{NO_3}$ constraints, $\gamma_{ss}(\mathrm{N_2O_5})$ deviation from true value increase dramatically, though the $\mathrm{NO_3}$-$\mathrm{N_2O_5}$ system behave generally closer to steady state. A larger deviation of $\gamma_{ss}(\mathrm{N_2O_5})$ will be yielded from linear fit at a higher $k\mathrm{NO_3}$ level, while the relative varieties of $k\mathrm{NO_3}$ stay the same. It indicates that the region with strong biogenic emissions is not suited to steady state fitting, such as TZ site, neither are the time periods with NO injection due to the resulted high reactivity and fast variation. Therefore, air mass with medium to low level of $k\mathrm{NO_3}$ is required to produce accurate $\gamma_{ss}(\mathrm{N_2O_5})$ when applying stead state to analysis, like data sets of airborne or residual measurements (Brown et al., 2009;Brown et al., 2006;Morgan et al., 2015).

Similarly, the influence of different levels of $k\mathrm{N_2O_5}$ is also explored by adjusting the pre-set $\gamma(\mathrm{N_2O_5})$ or the Sa concentration constraint in the steady state model, as presented in the Figure S9(c)&(d). With the enhancement of $k\mathrm{N_2O_5}$ level up to 5 times (Mod4), 12.5 times (Mod5) and 25 times (Mod6) of that in Mod0, the steady state approach can provide more reliable results of $\gamma_{ss}(\mathrm{N_2O_5})$, especially in the summer data set. This is because a large $k\mathrm{N_2O_5}$ level contributes to approaching steady state, which instinctively attenuates the deviation of fitting results produced by the small difference between both sides of Eq. (2).

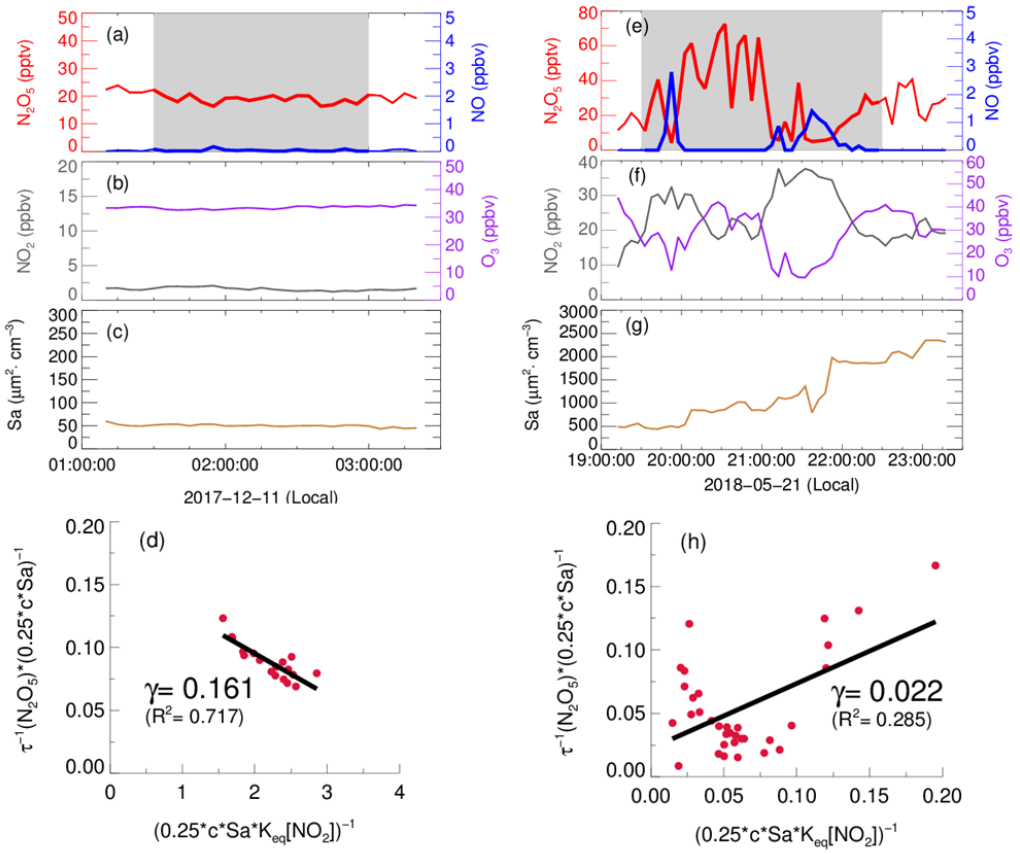

196

197 **Figure S1.** Exemplary steady state fit and the variations of relevant parameters in ambient conditions of
198 (a)&(b)&(c)&(d) PKU site and (e)&(f)&(g)&(h) TZ site. The red dots in (d)&(h) represent the plot of
199 $\left(0.25cS_a\tau_{ss}(\mathrm{N_2O_5})\right)^{-1}$ and $\left(0.25cS_aK_{eq}[\mathrm{NO_2}]\right)^{-1}$ used for fitting as illustrated in the method. The text on the
200 plot gives the best fit results of $\gamma(\mathrm{N_2O_5})$ and correlation coefficient.

201

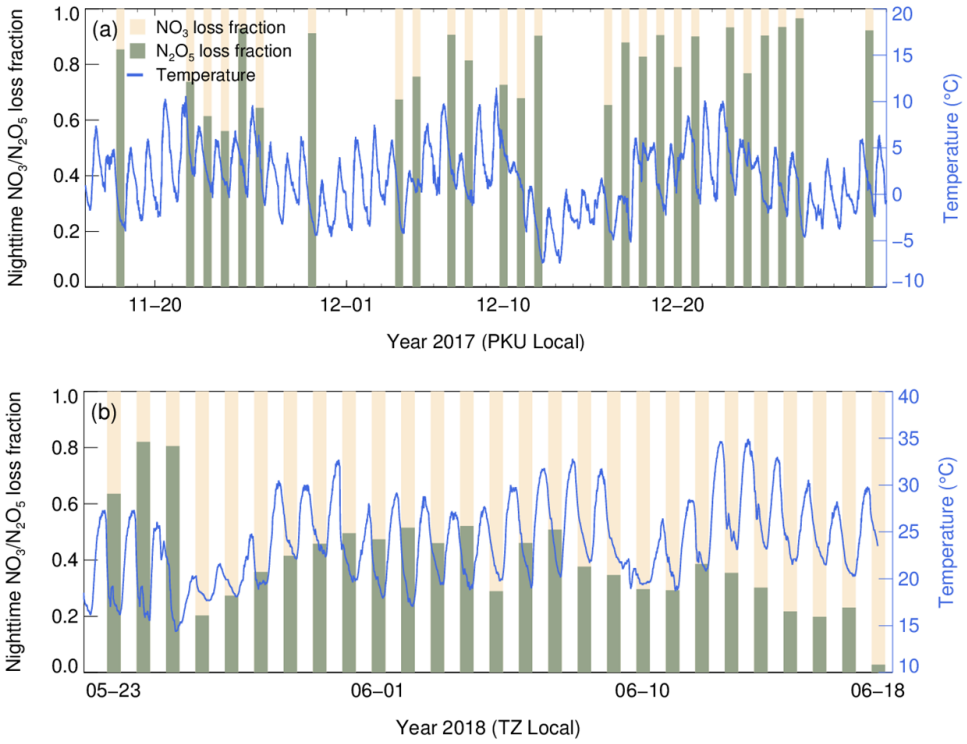

202

203 **Figure S2.** Timeseries of each night (SZA>90°) mean NO_3/N_2O_5 loss pathways fractions calculated from steady
204 state model and ambient temperature in (a) PKU2017 winter campaign and (b) TZ2018 summer campaign.

205

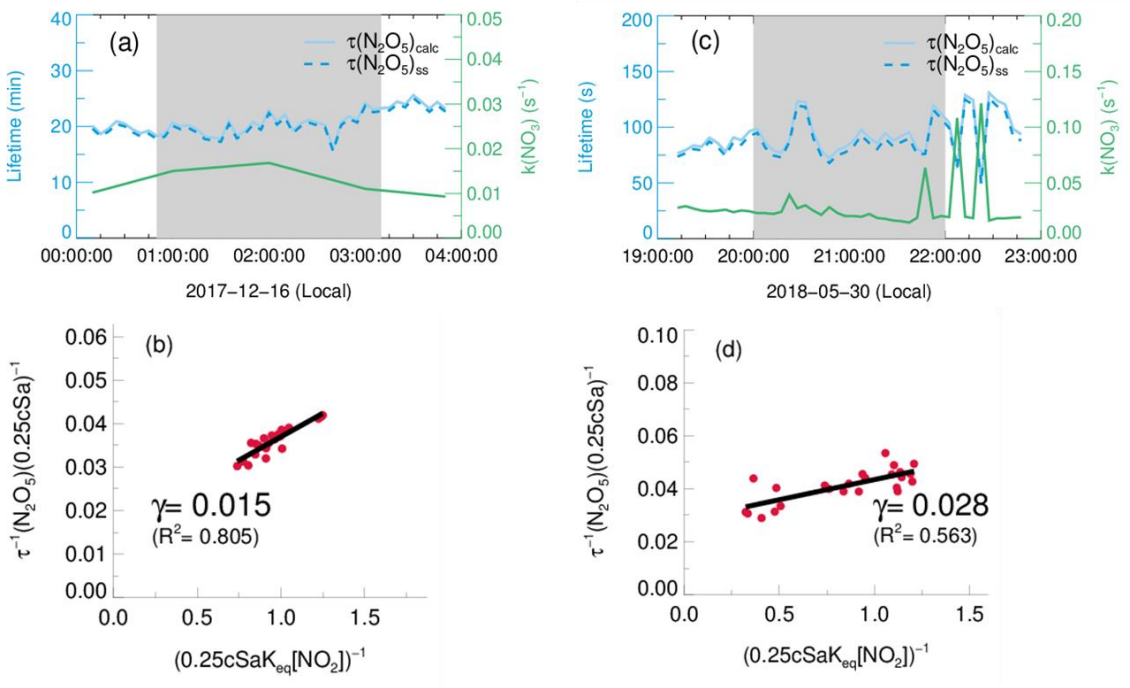

206

207 **Figure S3.** Example analysis of N_2O_5 lifetime and $\gamma_{ss}(N_2O_5)$ derivation through steady state fitting for (a)&(b)
208 PKU2017 case in winter and (c)&(d) TZ2018 case in summer. The steady state lifetime and calculated
209 atmospheric lifetime are shown as blue dash line and full line respectively. The green line is lumped NO_3 loss
210 frequency. The red dots in (b)&(d) represent data points in the shadow area, used for steady state fit (black line)
211 by the plot of $\left(0.25cS_a\tau_{ss}(N_2O_5)\right)^{-1}$ against $\left(0.25cS_aK_{eq}[NO_2]\right)^{-1}$. The text on the plot gives the best fit
212 results of $\gamma_{ss}(N_2O_5)$ and correlation coefficient.

213

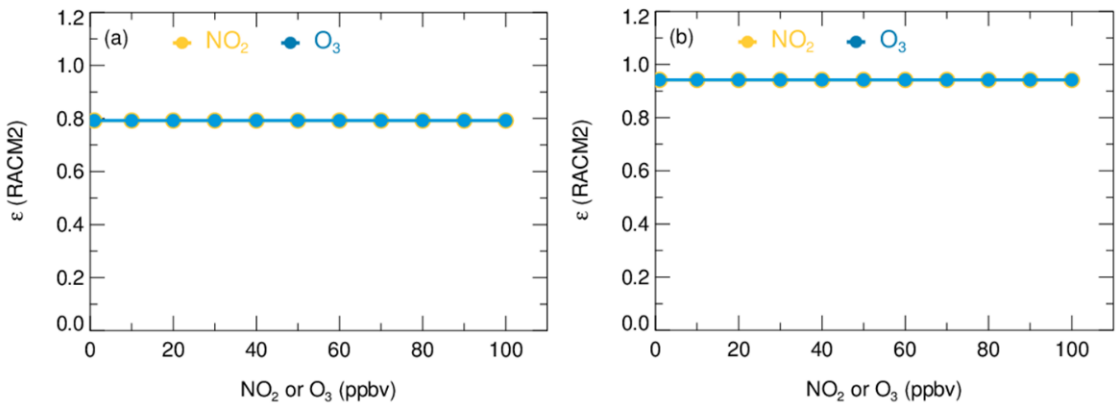

214

215 **Figure S4.** Sensitivity plot of NO_2 and O_3 concentration against coefficient ε calculated based on rate constants
216 from RACM2. (a) Initial model constraint is according to winter condition of PKU2017; (b) Initial model
217 constraint is according to summer condition of TZ2018.

218

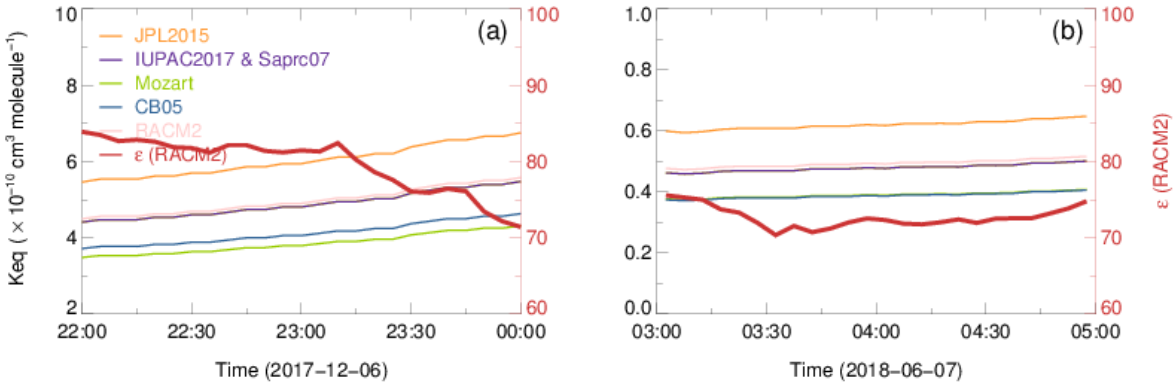

Figure S5. Exemplary comparison of *K*eq parameterization in (a) 2017-12-06 of PKU2017 dataset and (b) 2018-06-07 of TZ2018 dataset, using parameters from JPL2015 (orange), IUPAC2017&Saprc07 (purple), Mozart (green), CB05 (blue) and RACM2 (pink). It should be noted that the databases of Saprc07 and IUPAC2017 have the exactly same parameters, *K*eq derived from which are thus both denoted as purple line. The ε value calculated based on RACM2 is shown as red line.

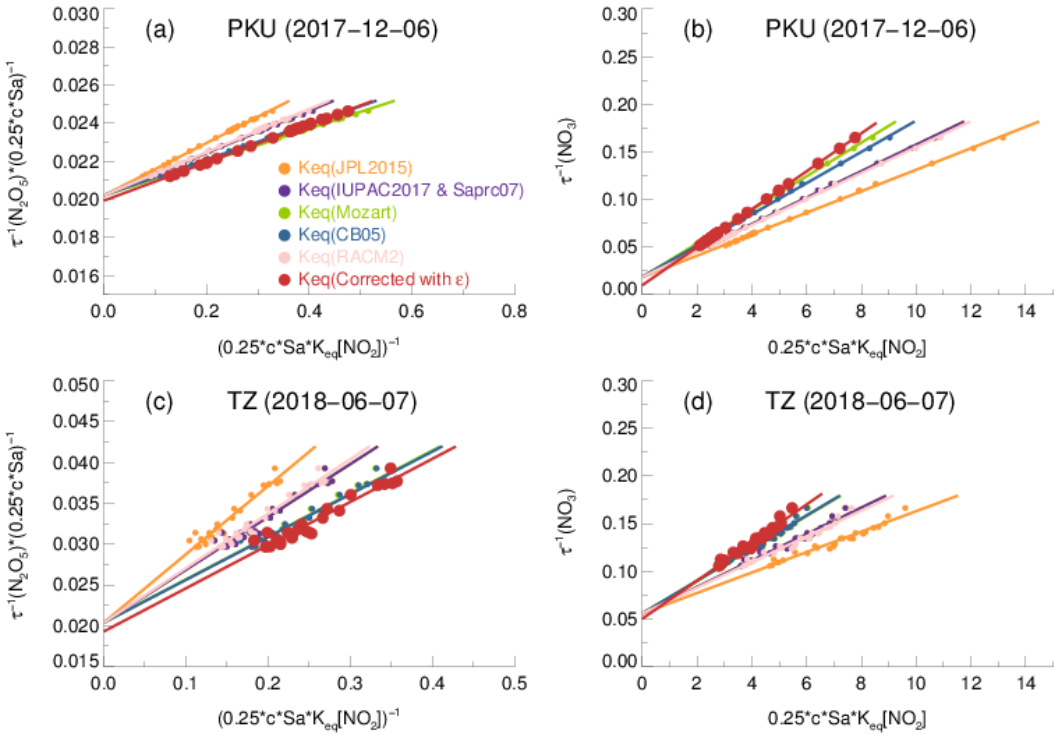

225

226 **Figure S6.** Exemplary fitting plot according to steady state approximation Eq. (1) (a)&(c) and Eq. (2) (b)&(d),
227 using *K*eq parameterization of JPL2015 (orange), IUPAC2017&Saprc07 (purple), Mozart (green), CB05 (blue)
228 and RACM2 (pink). The *K*eq (corrected by ε) is derived from output of steady state model coupled with RACM2.

229

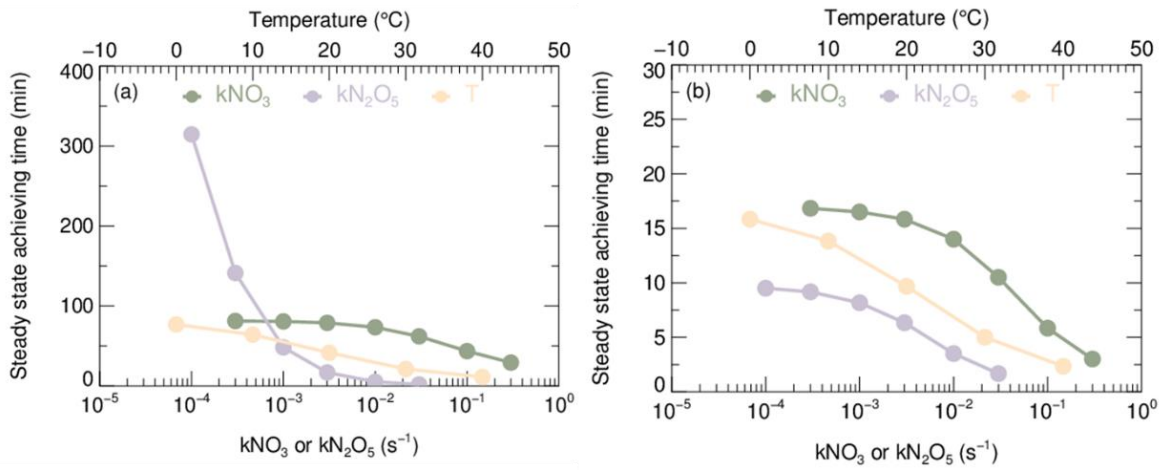

230

231 **Figure S7.** Sensitivity plot of $k\mathrm{NO_3}$, $k\mathrm{N_2O_5}$ and T against steady state achieving time of $\mathrm{NO_3}$-$\mathrm{N_2O_5}$ system. (a)
232 Initial model constraint is according to winter condition of PKU2017; (b) Initial model constraint is according to
233 summer condition of TZ2018.

234

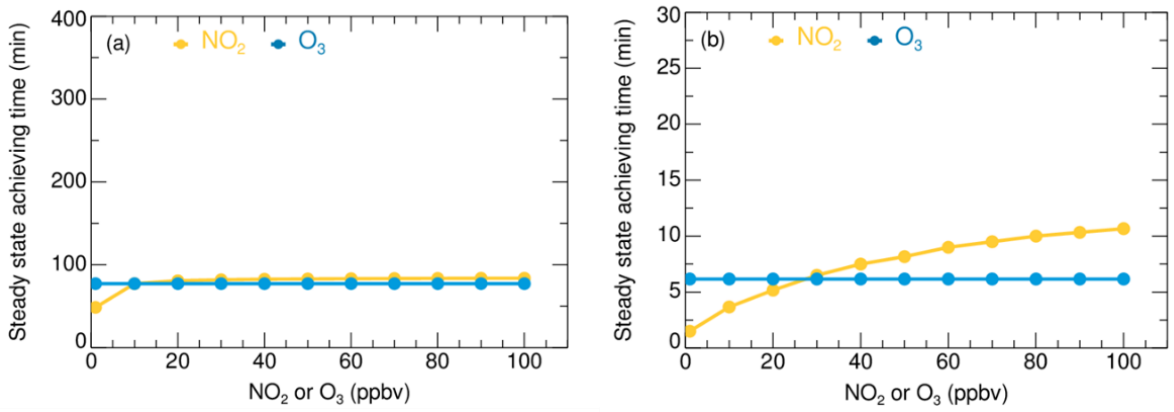

235

236 **Figure S8.** Sensitivity plot of NO_2 and O_3 concentration against steady state achieving time of NO_3-N_2O_5 system.

237 (a) Initial model constraint is according to winter condition of PKU2017; (b) Initial model constraint is according

238 to summer condition of TZ2018.

239

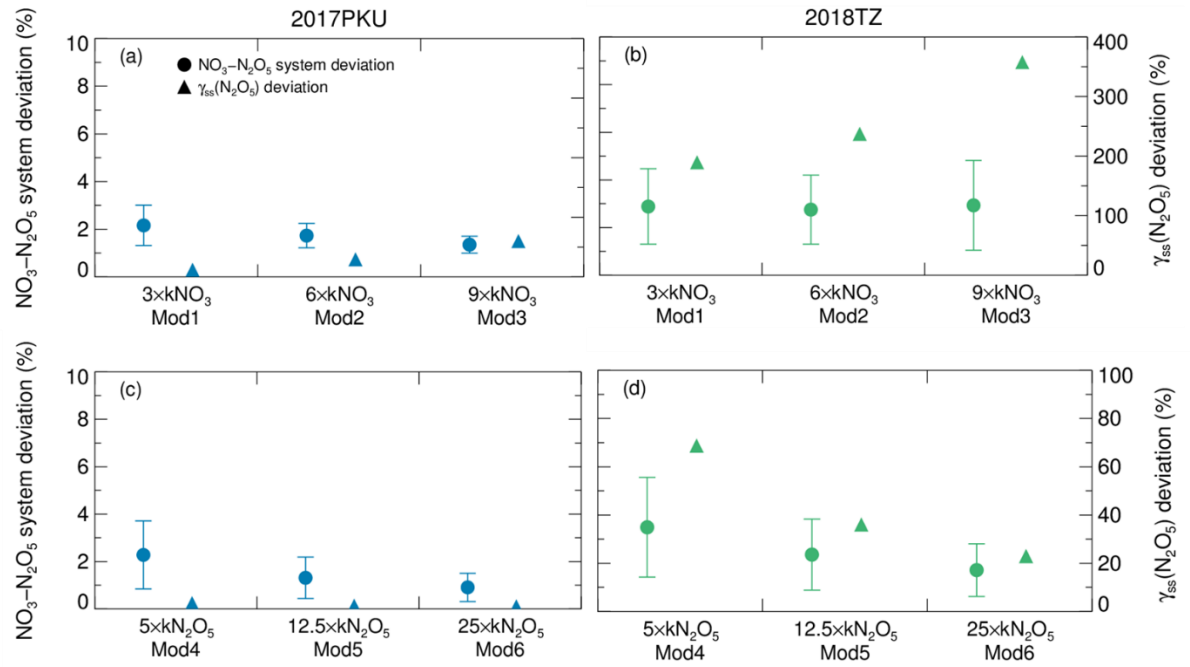

Figure S9. The average of NO_3-N_2O_5 system deviating from steady state and the median value of $\gamma_{ss}(N_2O_5)$ deviating from true value determined from different model constraints based on (a)&(c) PKU2017 dataset in blue and (b)&(d) TZ2018 dataset in green. The full circles represent the average of NO_3-N_2O_5 system deviating from steady state and the triangles represent the median deviation of $\gamma_{ss}(N_2O_5)$. As indicated in the text, the $k NO_3$ of Mod1, Mod2 and Mod3 are multiplied by 3,6 and 10 respectively against Mod0, and the $k N_2O_5$ of Mod4, Mod5 and Mod6 are multiplied by 5, 12.5 and 25 respectively against Mod0.

Table S1. Principal parameters and performance of related instruments.

Parameter	Technique	Time resolution	Detection Limit(1σ)	Accuracy
NO	Chemiluminescence[a]	1 min	200 pptv	±20%
NO_2	Chemiluminescence	1 min	300 pptv	±20%
O_3	UV photometry	1 min	500 pptv	±5%
VOCs	GC-MS/FID[b]	60 min	20-300 pptv	±15%
Monoterpene	PTR-MS[c]	10 s	20 ppyv	±15%
Sa	Nano SMPS, SMPS, APS	5 min	-	±10%

[a] Photolytic conversion to NO through blue light before detection; [b] Gas chromatography equipped with a mass spectrometer and a flame ionization detector; [c] Monoterpene was only measured in TZ2018.

252 **Table S2.** Parameters of initial model constraint for sensitivity test.

Parameters	NO_2/ppbv	O_3/ppbv	T/K	Sa/$\mu m^2 \cdot cm^{-3}$	$\gamma(N_2O_5)$[a]	kNO_3/s^{-1}
Winter case	10	23	276	540	0.02	9×10^{-3}
Summer case	27	49	300	2670	0.02	9×10^{-2}

253 [a.] With the Sa, T and $\gamma(N_2O_5)$, the constraint of kN_2O_5 can be calculated as 6×10^{-4} s^{-1} for winter case and 3×10^{-3} s^{-1} for summer case.

254

255 **Table S3.** Summary of parameters for calculating rate constant of k_{R1a}.

Source	k_0^{300}	n	k_∞^{300}	m	F	g
JPL2015	2.4×10^{-30}	3.0	1.6×10^{-12}	-0.1	0.6	1.0
Mozart	2.0×10^{-30}	4.4	1.4×10^{-12}	0.7	0.6	1.0
CB05	2.0×10^{-30}	4.4	1.4×10^{-12}	0.7	0.6	1.0
Saprc07	3.6×10^{-30}	4.1	1.9×10^{-12}	-0.2	0.35	$0.75\text{-}1.27\times\log_{10}0.35$
RACM2	2.0×10^{-30}	4.4	1.4×10^{-12}	0.7	0.6	1.0
IUPAC2017	3.6×10^{-30}	4.1	1.9×10^{-12}	-0.2	0.35	$0.75\text{-}1.27\times\log_{10}0.35$

256

257

Table S4. Summary of parameters for calculating rate constant of k_{R1b}.

Source	k_0^{300}	n	k_∞^{300}	m	F	g	A	B_1	B_2
JPL2015 [a]	2.4×10^{-30}	3.0	1.6×10^{-12}	-0.1	0.6	1.0	5.8×10^{-27}	10840	10840
Mozart	2.2×10^{-30}	4.4	1.4×10^{-12}	0.7	0.6	1.0	3.0×10^{-27}	10900	10900
CB05 [b]	k_0^{300}/A= 1.0×10^{-3}	3.5	k_∞^{300}/A= 9.7×10^{14}	-0.1	0.45	1.0	-	11000	11080
Saprc07 [b]	k_0^{300}/A= 1.3×10^{-3}	3.5	k_∞^{300}/A= 9.7×10^{14}	-0.1	0.35	0.75-$1.27\times\log_{10}0.35$	-	11000	11080
RACM2	2.2×10^{-30}	4.4	1.4×10^{-12}	0.7	0.6	1.0	2.7×10^{-27}	11000	11000
IUPAC2017 [b]	k_0^{300}/A= 1.3×10^{-3}	3.5	k_∞^{300}/A= 9.7×10^{14}	-0.1	0.35	0.75-$1.27\times\log_{10}0.35$	-	11000	11080

a. This rate constant expression is reformed from k_{R1a}/Keq as defined in JPL2015, where the k_{R1a} and Keq are calculated with values recommended by JPL2015;

b. The k_0^{300}/A and k_∞^{300}/A are given in the form of ratio instead of separately.

References:

Brown, S. S., Stark, H., and Ravishankara, A. R.: Applicability of the steady state approximation to the interpretation of atmospheric observations of NO3 and N2O5, J. Geophys. Res.- Atmos., 108, 10.1029/2003jd003407, 2003.

Brown, S. S., Ryerson, T. B., Wollny, A. G., Brock, C. A., Peltier, R., Sullivan, A. P., Weber, R. J., Dube, W. P., Trainer, M., Meagher, J. F., Fehsenfeld, F. C., and Ravishankara, A. R.: Variability in nocturnal nitrogen oxide processing and its role in regional air quality, Science, 311, 67-70, 10.1126/science.1120120, 2006.

Brown, S. S., Dube, W. P., Fuchs, H., Ryerson, T. B., Wollny, A. G., Brock, C. A., Bahreini, R., Middlebrook, A. M., Neuman, J. A., Atlas, E., Roberts, J. M., Osthoff, H. D., Trainer, M., Fehsenfeld, F. C., and Ravishankara, A. R.: Reactive uptake coefficients for N2O5 determined from aircraft measurements during the Second Texas Air Quality Study: Comparison to current model parameterizations, J. Geophys. Res.- Atmos., 114, D00F10(01-16), Artn D00f10

10.1029/2008jd011679, 2009.

Cantrell, C., Davidson, J., McDaniel, A., Shetter, R., and Calvert, J.: The equilibrium constant for N2O5 = NO2 + NO3 - Absolute determination by direct measurement from 243 to 397 K, The Journal of Chemical Physics, 88, 10.1063/1.454679, 1988.

Cantrell, C., Shetter, R., Calvert, J., Tyndall, G., and Orlando, J.: Measurement of rate coefficients for the unimolecular decomposition of N2O5, The Journal of Physical Chemistry, 97, 10.1021/j100138a013, 1993.

Graham, R., and Johnston, H.: The photochemistry of the nitrate radical and the kinetics of the nitrogen pentoxide-ozone system, The Journal of Physical Chemistry, 82, 10.1021/j100492a002, 1978.

Kircher, C., Margitan, J., and Sander, S.: Pressure and temperature dependence of the reaction nitrogen dioxide + nitrogen trioxide + M .fwdarw. nitrogen pentoxide (N2O5) + M, The Journal of Physical Chemistry, 88, 10.1021/j150663a037, 1984.

Ma, X., Tan, Z., Lu, K., Yang, X., Liu, Y., Li, S., Li, X., Chen, S., Novelli, A., Cho, C., Zeng, L., Wahner, A., and Zhang, Y.: Winter photochemistry in Beijing: Observation and model simulation of OH and HO2 radicals at an urban site, Sci. Total Environ., 685, 85-95, https://doi.org/10.1016/j.scitotenv.2019.05.329, 2019.

Morgan, W. T., Ouyang, B., Allan, J. D., Aruffo, E., Di Carlo, P., Kennedy, O. J., Lowe, D., Flynn, M. J., Rosenberg, P. D., Williams, P. I., Jones, R., McFiggans, G. B., and Coe, H.: Influence of aerosol chemical composition on N2O5 uptake: airborne regional measurements in northwestern Europe, Atmos. Chem. Phys., 15, 973-990, 10.5194/acp-15-973-2015, 2015.

Osthoff, H., Pilling, M., Ravishankara, A. R., and Brown, S.: Temperature Dependence of the NO3 Absorption Cross-section Above 298 K and Determination of the Equilibrium Constant for NO3 + NO2 N2O5 at Atmospherically Relevant Conditions, Physical chemistry chemical physics : PCCP, 9, 5785-5793, 10.1039/B709193A, 2007.

Pritchard, H.: The nitrogen pentoxide dissociation equilibrium, Int. J. Chem. Kinet., 26, 61-71, 10.1002/kin.550260108, 1994.

Smith, C., and Ravishankara, A. R.: Kinetics of the reaction nitrogen dioxide + nitrogen trioxide + M at low pressures and 298 K, The Journal of Physical Chemistry, 89, 10.1021/j100254a024, 1985.

Wang, H., Chen, X., Lu, K., Tan, Z., Ma, X., Wu, Z., Li, X., Liu, Y., Shang, D., Wu, Y., Zeng, L., Hu, M., Schmitt, S., Kiendler-Scharr, A., Wahner, A., and Zhang, Y.: Wintertime N2O5 uptake coefficients over the North China Plain, Science Bulletin, 65, 765-774, https://doi.org/10.1016/j.scib.2020.02.006, 2020.